

Critical temperature of a trapped, weakly interacting Bose gas

F. Gerbier,* J. H. Thywissen,† S. Richard, M. Hugbart, P. Bouyer, and A. Aspect
Groupe d'Optique Atomique, Laboratoire Charles Fabry de l'Institut d'Optique ‡, 91403 Orsay Cedex, France
(Dated: May 22, 2019)

We report on measurements of the critical temperature of a harmonically trapped, weakly interacting Bose gas as a function of atom number. We exclude ideal-gas behavior by more than two standard deviations, and find agreement with mean-field theory. We find no evidence for the presence of critical fluctuations, as would exist in a uniform gas. In the course of this measurement, the onset of hydrodynamic expansion in the thermal component has been observed. Our thermometry method takes this feature into account.

PACS numbers: 03.75.Fi, 03.75.-b, 05.30.Jp

Degenerate atomic Bose gases provide an ideal testing ground for the theory of quantum fluids. First, their diluteness makes possible first-principles theoretical approaches [1]. Second, thanks to the powerful experimental techniques of atomic physics, static and dynamic properties can be studied quantitatively through a wide range of temperature and densities. Furthermore, the inhomogeneity induced by the external trapping potential leads to entirely new behavior, when compared to bulk quantum fluids.

Atomic interactions have previously been found to affect deeply the dynamical behavior of trapped Bose gases at finite temperature [2, 3]. By contrast, the influence of interactions on *thermodynamics* is less pronounced [4], and has been less studied experimentally. Pioneering work on thermodynamics [5] concentrated essentially on the ground state occupation, and the role of interactions was somewhat hidden by finite size effects [1]. Though several such measurements have been reported [3, 6, 7, 8, 9], to our knowledge a decisive test of the role of interactions is still lacking. In this Letter, we focus on the critical temperature T_c of a harmonically trapped ^{87}Rb Bose gas to demonstrate the influence of interactions on the thermodynamics. We study the behavior of T_c as a function of the number of atoms at the transition, for a fixed trapping geometry. We find a deviation from ideal-gas behavior, towards lower critical temperatures, whose signification will be discussed below. In the course of this study, we have observed that, even far from the hydrodynamic regime [10, 11], collisions already induce an anisotropy in the free expansion of the cloud. We correct for this effect in the determination of the initial temperature.

In the thermodynamic limit [1], a trapped ideal gas undergoes Bose-Einstein condensation at a temperature

$$k_B T_c^0 = \hbar \bar{\omega} \left(\frac{N}{\zeta(3)} \right)^{1/3}, \quad (1)$$

with N the total atom number, ω_\perp and ω_z the trapping frequencies, $\bar{\omega} = \omega_\perp^{2/3} \omega_z^{1/3}$ their geometrical average, and ζ the Riemann zeta function. Finite-size effects smoothen the transition and reduce T_c . To leading order in $1/N$ (see [1] and references therein), one finds

$$k_B T_c^{\text{ideal}} = k_B T_c^0 - \frac{\zeta(2)}{6\zeta(3)} \hbar (\omega_z + 2\omega_\perp). \quad (2)$$

Two-body, repulsive interactions in the gas lower the critical temperature further, according to [4]

$$\frac{T_c - T_c^{\text{ideal}}}{T_c^0} \approx -\alpha N^{1/6}, \quad (3)$$

with the coefficient $\alpha \approx 1.326 a/\sigma$, where a is the s-wave scattering length, and $\sigma = \sqrt{\hbar/M\bar{\omega}}$ is the mean ground state width. The shift (3) can be understood using a simple mean-field picture [4]: interactions lower the density in the center of the trap $n(\mathbf{0})$, and accordingly decrease the temperature T that meets Einstein's criterion $n(\mathbf{0})\lambda_T^3 \approx \zeta(3/2)$, whith $\lambda_T = \sqrt{2\pi\hbar^2/Mk_B T}$ the thermal de Broglie wavelength. In this work, the finite-size correction in Eq. (2) changes T_c^0 by at most 2%, whereas the interactive shift (3) can be as high as 10%.

Critical fluctuations, as discussed in [4, 12, 13], may also affect the behavior of the system near the transition, as for the case of an uniform Bose gas. Indeed, in the uniform case, the critical temperature is not affected at the mean-field level. The leading correction is due to critical, long-wavelength density fluctuations that are predicted to *increase* T_c ([12, 14] and references therein). Such an upwards trend has been observed experimentally in a dilute sample of ^4He adsorbed on Vycor [15]. In contrast, the quantitative agreement we find with the mean-field result (3) implies that this effect is suppressed in a trapped gas. This observation, in line with the theoretical arguments put forward in [4, 12], highlights the important role played by the trapping potential in suppressing very long wavelength excitations.

Our experimental setup to reach Bose-Einstein condensation in the $|F = 1; m_F = -1\rangle$ hyperfine ground state of ^{87}Rb is similar to that used in [16]. The trapping frequencies are $\omega_\perp/2\pi = 413(5)$ Hz and $\omega_z/2\pi = 8.69(2)$ Hz in

*UMR 8501 du CNRS

the present work. To reduce non-equilibrium shape oscillations that occur in such anisotropic traps upon condensation [11, 16], the last part of the evaporation ramp is considerably slowed down (to a ramp speed of 200 kHz/s) and followed by a 1 s hold time in the presence of a radio-frequency shield. We ensure good reproducibility of the evaporation ramp in the following way. We monitor regularly (typically every four cycles) the radio-frequency ν_0 that empties the trap. This allows us to detect slow drifts of the trap bottom, and to adjust in real time the final evaporation radio-frequency ν_{rf} to follow them. In this way, the “trap depth” $\nu_{\text{rf}} - \nu_0$, is kept constant within ± 2 kHz. Since we measure $\eta = h(\nu_{\text{rf}} - \nu_0)/k_{\text{B}}T \approx 11$ in this final evaporation stage, we estimate the temperature stability to be ± 10 nK.

We infer the properties of the clouds by absorption imaging. After rapid switch-off of the trap ($1/e$ cut-off time of about 50 μs), a 22.3 ms free expansion, and a repumping pulse, we probe the ultra-cold cloud on resonance with the $|F = 2\rangle \rightarrow |F' = 3\rangle$ transition [17]. The images are analyzed using a standard procedure, described for instance in [18]. For an ideal thermal cloud above the transition point, the evolution of the density in time of flight is related to the initial density profile by simple scaling relations, so that the column density (integrated along the probe line-of-sight, almost perpendicular to the long axis of the trap) is

$$\tilde{n}_{\text{th}}(\rho) = \tilde{n}_{\text{th}}(0)g_2 \left\{ \exp \left(\frac{\mu}{k_{\text{B}}T} - \frac{x^2}{2R_{\text{th}}^2} - \frac{z^2}{2L_{\text{th}}^2} \right) \right\} \quad (4)$$

with x the coordinate along the tight trapping axis, z along the shallow one, and $g_2(u) = \sum_{j \geq 1} u^j / j^2$. For mixed clouds containing a normal and a (small) condensed component, we assume, as usual for a condensate in the Thomas-Fermi regime [1], that one can describe the bimodal distribution by an inverted parabola on top of an ideal, quantum-saturated thermal distribution (Eq. (4) with $\mu = 0$). The condensed number N_0 is then deduced from integration of the Thomas-Fermi fit, and the total atom number N from integration over the entire image. We estimate that condensed fractions of 1% or higher can be reliably detected by the fitting routine. Absolute accuracy on the value of N and N_0 relies on the precise knowledge of the absorption cross-section of the probe laser, which depends on its polarization and the local magnetic field. This cross-section is calibrated by fitting the radial sizes of condensates with no discernible thermal fraction to the Thomas-Fermi law $R_0 \propto N_0^{1/5}$, as explained in [1, 10, 18, 19]. We find a reduction of 4.00(14) compared to the reference value $\sigma_0 = 3\lambda_{\text{L}}^2/2\pi$ [17].

We will now discuss the more complex issue of thermometry in some detail. The temperature is usually inferred from the sizes of the thermal cloud after a time of flight t , assuming a purely ballistic expansion with

isotropic mean velocity, $v_0 = \sqrt{k_{\text{B}}T/M}$, as appropriate for an ideal gas. We show in Fig. 1 that the observed aspect ratio of non-condensed clouds, in a wide range of temperatures and atom numbers (corresponding to $1 \lesssim T/T_c \lesssim 1.8$), is actually larger than the value (0.773) expected for an ideal gas and $\omega_z t \approx 1.23$ that corresponds to our parameters (dotted line in Fig. 1). This implies a radial expansion faster than the axial one, in contradiction with the assumption of an isotropic velocity distribution.

In a very elongated trap, this could be explained by two distinct collisional effects. First, the mean-field energy of the non-degenerate cloud distorts the equilibrium density profile [20], and converts almost completely into radial expansion energy during time-of-flight [21], as in an elongated condensate [10, 19]. The magnitude of these effects is controlled by the ratio χ of the mean-field energy to the temperature. In our case, the parameter χ does not exceed 0.02, too low to explain the observed anisotropy (dashed line in Fig. 1, calculated along the lines of [21]).

Second, as studied theoretically in [10, 22, 23] and observed in Bose [11] and Fermi gases [24], anisotropic expansion occurs for a cloud in the hydrodynamic regime, *i.e.* when the mean free path at equilibrium is smaller than the dimensions of the sample. Collisions in the initial stage of the expansion ($t \lesssim \omega_{\perp}^{-1}$) convert thermal motion along the shallow z axis into hydrodynamic motion in the two tightly confined directions. In our case, because of the large aspect ratio of the cloud, the mean free path is typically smaller than the axial length, but much larger than the radial size. In this situation, one expects a weak deviation from collisionless behavior, and (for $t \gg \omega_{\perp}^{-1}$) mean square expansion velocities of the form $\langle v_x^2 \rangle / v_0^2 \approx 1 + \beta \gamma_{\text{coll}} / 2\omega_{\perp}$, and $\langle v_z^2 \rangle / v_0^2 \approx 1 - \beta \gamma_{\text{coll}} / \omega_{\perp}$, with γ_{coll} the collision rate at thermal equilibrium and β a coefficient, that depends in general on $\omega_{\perp}, \omega_z, t$ (fixed for the measurement presented here). The aspect ratio is thus expected to increase linearly with γ_{coll} , in agreement with the trend observed in Fig 1.

In [23], a set of scaling equations was derived to investigate how mean-field and collisions affect the expansion of a non-condensed cloud. The prediction of a numerical solution of these equations, shown by the solid line in Fig. 1, agrees satisfactorily with our data, and supports the arguments presented above. This calculation makes use of the results of [25] for the collision rate of a Bose gas, in general larger (by as much as 70% close to T_c) than the classical collision rate with the same N and T [26]. In view of the satisfactory agreement of our data with the scaling theory, we conclude that the observed anisotropy is a signature of the onset of hydrodynamic expansion.

In the regime $\gamma_{\text{coll}} \lesssim \omega_{\perp}$, where the anisotropy is weak and increases linearly with γ_{coll} , it is straightforward to correct experimentally for these hydrodynamic effects,

provided the expansion velocity along both axes is measured [27]. Were this correction not applied, a systematic 10-15% discrepancy between the axial and radial temperature would remain. Note that mean-field effects are not corrected by this procedure. As stated above, they change the expansion energy by 2% at most. This error is not significant when compared to calibration uncertainties, that limit the accuracy on T to about 5%.

Having identified an appropriate thermometric technique, we turn to the measurement of the critical temperature as a function of atom number. Data were taken in a narrow range around T_c . From the two-component fit, we extract the number of condensed atoms, the temperature, and the total atom number as a function of the trap depth, as shown in Fig. 2a, b and c, respectively. The trap depth at which the transition point is reached, $(\nu_{\text{rf}} - \nu_0)_c$, is taken to be the point at which a linear fit to the condensed number data crosses zero (a linear approach towards T_c is consistent with the simulations reported in [28]). The temperature and total number are also fitted assuming a linear dependency on ν_{rf} , and from the value $(\nu_{\text{rf}} - \nu_0)_c$, we extract the critical atom number N_c and critical temperature T_c .

In Fig. 3, we have plotted T_c as a function of N_c , measured in ten independent data sets. The ideal gas value T_c^{ideal} (dashed line) lies two standard deviations above our data. Including the mean-field correction (3) yields a much better agreement (solid line). To quantify our measurement, we have assumed a form $-\alpha N^{1/6}$ for the interactive shift in T_c , with a free coefficient α . We find $\alpha = 0.009(1)^{+0.002}_{-0.001}$, whereas Eq. (3) predicts $\alpha \approx 0.007$ for a scattering length $a \approx 5.31 \text{ nm}$ [29] and $\sigma \approx 1.00 \mu\text{m}$. The first uncertainty quoted is statistical, while the upper and lower bounds reflect calibration uncertainties and the estimated error in finding the point where N_0 goes to zero. The shaded area in Fig. 3 delineates the resulting confidence interval.

The data shown in Fig. 3 reasonably exclude any additional shift of the same order of magnitude as (3). In particular, if there were a critical shift in T_c similar to the one predicted in the uniform case [14], one would expect instead $\alpha \approx 0.004$, a value not consistent with our findings within the estimated accuracy. This observation is in line with the predicted suppression of critical density fluctuations in a trapped system compared to the uniform case [4, 12]. Indeed, in the presence of the inhomogeneous potential, long-wavelength critical fluctuations, responsible for the first-order shift, are strongly suppressed. Short-wavelength fluctuations are still present, but can only provide a second-order in $a/\lambda_{T_c^0}$ correction to Eq. (3). For our experimental situation, we calculate from [12] an additional upwards shift in T_c smaller than 1%, below the sensitivity of the measurement.

In summary, we have measured the critical temperature of a trapped, weakly-interacting Bose gas. Our results exclude ideal gas behavior by two standard de-

viations, and we find satisfactory agreement with mean-field theory. We find no evidence for critical behavior close to T_c within our experimental sensitivity, in line with recent theoretical estimates [4, 12]. In addition, we have observed hydrodynamic behavior in the expansion of the thermal cloud, and shown how to correct for it in the thermometry procedure. Below T_c , the presence of the condensate changes the picture presented here significantly. The static and dynamic behavior of a mixed cloud, in particular in free expansion, remains to a large extent an open problem, that we will address in a separate publication [30]. We note to conclude that measuring corrections to T_c beyond the mean-field for our experimental parameters would require thermometry with an accuracy of 1% or better. Alternatively, these many-body effects could be enhanced in the vicinity of a Feshbach resonance [31].

We acknowledge useful discussions with D. Guéry-Odelin concerning the work reported in [23]. We also thank D. Boiron, J. Retter, J. Dalibard and S. Giorgini for useful comments on this work. JHT acknowledges support from CNRS, and MH from IXSEA. This work was supported by DGA, and the European Union.

* email: fabrice.gerbier@iota.u-psud.fr

† current address: Department of Physics, University of Toronto, Toronto, ON, M5S 1A7, Canada.

- [1] F. Dalfovo, S. Giorgini, L. P. Pitaevskii, S. Stringari, Rev. Mod. Phys. **71**, 463 (1999).
- [2] D. S. Jin *et al.*, Phys. Rev. Lett. **78**, 764 (2001); D. Stamper-Kurn *et al.*, Phys. Rev. Lett. **81**, 500 (1998); F. Chevy *et al.*, Phys. Rev. Lett. **88**, 250402-1 (2002).
- [3] O. Maragò, G. Hechenblaikner, E. Hodby, C. Foot, Phys. Rev. Lett. **86**, 3938 (2001).
- [4] S. Giorgini, L. Pitaevskii, S. Stringari, Phys. Rev. A **54**, R4633 (1996); J. Low Temp. Phys. **109**, 309 (1997).
- [5] J. Ensher *et al.*, Phys. Rev. Lett. **77**, 4984 (1996).
- [6] M.-O. Mewes *et al.*, Phys. Rev. Lett. **77**, 416 (1996).
- [7] D. J. Han, R. H. Wynar, Ph. Courteille, D. J. Heinzen, Phys. Rev. A **57**, R4114 (1998).
- [8] B. Anderson, M. Kasevich, Phys. Rev. A **59**, R938 (1999).
- [9] F. Schreck *et al.*, Phys. Rev. Lett. **87**, 080403 (2001).
- [10] Y. Kagan, E. Surkov, G. Shlyapnikov, Phys. Rev. A **55**, R18 (1997).
- [11] I. Schvarchuck *et al.*, Phys. Rev. Lett. **89**, 270404 (2002).
- [12] P. Arnold, B. Tomášik, Phys. Rev. A **64**, 053609 (2001).
- [13] M. Houbiers, H. T. C. Stoof, E. A. Cornell, Phys. Rev. A **56**, 2041 (1997).
- [14] P. Grüter, D. Ceperley, F. Laloë, Phys. Rev. Lett. **79**, 3549 (1997); G. Baym *et al.*, Phys. Rev. Lett. **83**, 1703 (1999); G. Baym, J.-P. Blaizot, J. Zinn-Justin, Euro. Phys. Lett. **49**, 150 (2000); P. Arnold, G. Moore, Phys. Rev. Lett. **87**, 120401 (2001); V. A. Kashurnikov, N. Prokof'ev, B. Svistunov, Phys. Rev. Lett. **87**, 120402 (2001); M. Holzmann *et al.*, Phys. Rev. Lett. **87**, 120403 (2001).

[15] J. D. Reppy *et al.*, Phys. Rev. Lett. **84**, 2060 (2000).

[16] S. Richard *et al.*, Phys. Rev. Lett. **91**, 010405 (2003).

[17] The probe laser wavelength is $\lambda_L = 780.02$ nm; its intensity is 0.17 mW/cm 2 , and the imaging pulse length is $34\ \mu\text{s}$. The laser polarization is linear.

[18] W. Ketterle, D. S. Durfee, D. M. Stamper-Kurn, in *Proceedings of the International School of Physics - Enrico Fermi*, M. Inguscio, S. Stringari, and C.E. Wieman, eds. (IOS Press, 1999).

[19] Y. Castin, R. Dum, Phys. Rev. Lett. **77**, 5315 (1996).

[20] D. Guéry-Odelin, Phys. Rev. A **66**, 033613 (2002).

[21] C. Menotti, P. Pedri, S. Stringari, Phys. Rev. Lett. **89**, 250402 (2002).

[22] H. Wu, E. Arimondo, Europhys. Lett. **43**, 141 (1998).

[23] P. Pedri, D. Guéry-Odelin, S. Stringari, cond-mat/0305624.

[24] K. M. O'Hara *et al.*, Science **298**, 2179 (2002); C. A. Regal, D. S. Jin, Phys. Rev. Lett. **90**, 230404 (2003); T. Bourdel *et al.*, to appear in Phys. Rev. Lett. (2003).

[25] G. M. Kavoulakis, C. J. Pethick, H. Smith, Phys. Rev. A **61**, 053603 (2000).

[26] The results derived in [25] for γ_{coll} are well reproduced by the formula $\gamma_{\text{coll}} \approx \gamma_{\text{class}}(1 + 0.23/t^3 + 0.4/t^4)$,

with $t = T/T_c^0$. Following [23], we define the collision rate for a *classical* gas as $\gamma_{\text{class}} = 2n_{\text{class}}(\mathbf{0})\sigma_{\text{el}}v_{\text{th}}/5$, with $\sigma_{\text{el}} = 8\pi a^2$ the s-wave cross-section, $n_{\text{class}}(\mathbf{0}) = N\bar{\omega}^3(m/2\pi k_{\text{B}}T)^{3/2}$ the classical peak density and $v_{\text{th}} = \sqrt{8k_{\text{B}}T/\pi M}$.

[27] In practice, we deduce effective temperatures from the measured sizes R_i of the cloud ($i = x, z$), according to $k_{\text{B}}T_i = M\omega_i^2 R_i^2/b_i^2$, with $b_i = (1 + \tau_i^2)^{1/2}$ and $\tau_i = \omega_i t$. We infer the initial temperature T_0 from T_x and T_z using the linear combination $T_0 \approx 2\tau_z^2/(1 + 3\tau_z^2)T_x + (1 + \tau_z^2)/(1 + 3\tau_z^2)T_z$, that cancels the hydrodynamic corrections to first order in $\gamma_{\text{coll}}/\omega_{\perp}$.

[28] M. Holzmann, W. Krauth, M. Naraschewski, Phys. Rev. A **59**, 2956 (1999); T. Bergeman, D. L. Feder, N. L. Balasz, B. I. Schneider, Phys. Rev. A **61**, 063605 (2000).

[29] E. G. M. van Kempen, S. J. J. M. F. Kokkelmans, D. J. Heinzen, B. J. Verhaar, Phys. Rev. Lett. **88**, 093201 (2002).

[30] F. Gerbier *et al.*, in preparation (2003).

[31] S. Inouye *et al.*, Nature **392**, 151 (1998); S. Cornish *et al.*, Phys. Rev. Lett. **85**, 1795 (1998).

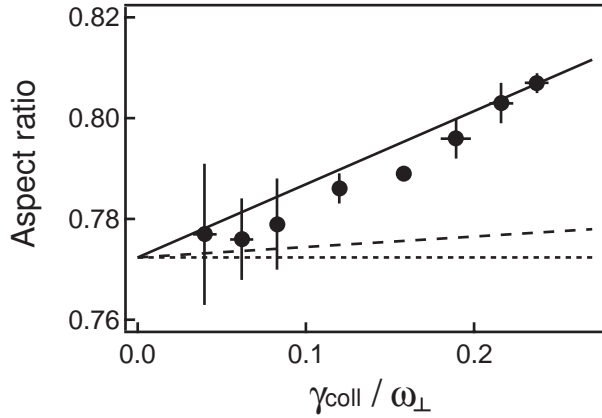


FIG. 1: Onset of hydrodynamic expansion for trapped clouds above threshold. Measured aspect ratios after expansion (filled circles, with statistical error bars) are plotted versus the collision rate at equilibrium γ_{coll} . The experimental results are compared against several hypotheses: a ballistic expansion (dotted line); a mean-field dominated expansion (dashed line); and a collisional expansion for a non-condensed Bose gas (solid line). Note that the calculations shown have no free parameters, since they depend only on N and T that are both measured.

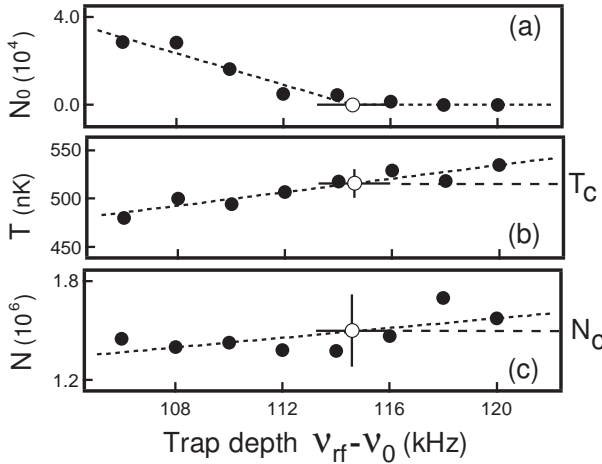


FIG. 2: Procedure to locate the transition point. We plot the condensed number (a), temperature (b), and total atom number (c) as a function of the trap depth, fixed by the final rf frequency ν_{rf} and the trap bottom ν_0 . The transition point, shown as a hollow circle (with statistical error bars), is found from a fit [dotted curve in (a)], and reported in (b) and (c) to find T_c and N_c .

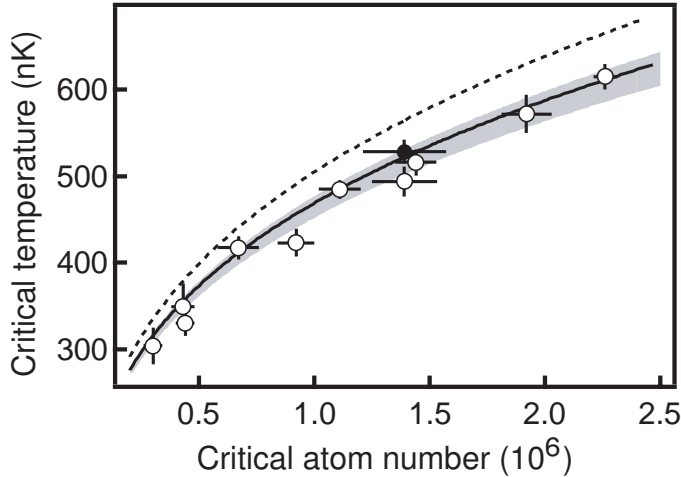


FIG. 3: Critical temperature as a function of atom number at the transition. The experimental points (circles) are lower than the ideal gas law Eq. (1) (dashed) by at least two standard deviations. The observed decrease of T_c is consistent with a mean-field shift given by Eq. (3) (solid line). Error bars indicate the statistical dispersion, and the shaded area the possible range of fits including calibration uncertainties. The filled circle represents the data of Fig. 2.